Publishing Excellence Inspiring Progress
ARISTON PUBLICATIONS
MatSci Express
ISSN: 2997-8440 www.aristonpubs.com/matsci-express https://doi.org/10.69626/mse.2025.0237

RESEARCH ARTICLE

Tuning the Structural, Electrical, and Magnetic Properties of Nanocrystalline Copper Ferrite through Nickel Substitution

K. R. Sanadi [1,*], K. C. Rathod [2], A. S. Varale [3], V. G. Parale [4], R. R. Powar [5], A. V. Mali [6]

ABSTRACT: A comprehensive study on the synthesis and properties of nickel-substituted copper ferrite nanoparticles ($Cu_{1-x}Ni_xFe_2O_4$, where x = 0.0, 0.25, 0.50, 0.75, 1.0) is presented. These nanomaterials were successfully fabricated using a sol-gel auto-combustion technique, a method renowned for its cost-effectiveness and ability to produce homogenous, fine powders at relatively low temperatures. X-ray diffraction analysis confirmed the formation of a pure, single-phase cubic spinel structure for all compositions, with the average crystallite size being approximately 21 nm. Investigations into elemental composition using energy dispersive spectroscopy verified the intended stoichiometry, while scanning electron microscopy revealed the morphology and slight grain growth with increasing nickel content. Electrical resistivity measurements demonstrated semiconducting behavior across all samples, with resistivity decreasing as nickel content increased. Thermoelectric power analysis showed that all compositions exhibited n-type semiconductor characteristics, except for pure nickel ferrite (x=1.0), which displayed p-type behavior. Magnetic characterization via vibrating sample magnetometry confirmed the ferrimagnetic nature of the materials. A significant finding was the transformation from hard magnetic characteristics in copper-rich ferrites to softer magnetic properties in nickel-rich compositions, as evidenced by a reduction in coercivity. These tailored properties highlight the potential of these synthesized ferrites for advanced applications in electronics, including high-frequency magnetic cores, memory devices, and sensors.

Keywords: Nickel-copper ferrite, sol-gel combustion, nanocrystalline spinel, magnetic properties, semiconductor behavior, cation substitution.

Received: 20 February 2025; Revised: 15 May 2025; Accepted: 28 June 2025; Published Online: 15 July 2025

1. INTRODUCTION

The relentless advancement of modern technology, driven by demands for miniaturization and enhanced performance, has positioned functional nanomaterials at the center of scientific innovation [1]. Among these, nano-crystalline spinel ferrites stand out as a particularly compelling class of materials due to their remarkable and highly tunable electronic, magnetic, and catalytic properties [2]. These materials have transitioned from laboratory curiosities to indispensable components in a vast array of applications that define contemporary life [3-6]. The fundamental structure of these materials conforms to the general formula AB_2O_4, which consists of a closely packed face-centered cubic lattice of oxygen ions. Within this lattice, metal cations occupy two distinct types of interstitial sites: the tetrahedral (A-site) and octahedral (B-site) positions [7]. The specific identity and distribution of these cations between the two sites is the primary factor governing the resulting electrical and magnetic characteristics of the ferrite [8]. This distribution is not a fixed property but can be

[1] Department of Chemistry, Doodhsakhar Mahavidyalaya Bidri, Kolhapur-416208, India
[2] Department of Chemistry, The New College Kolhapur, Maharastra-416004, India
[3] Department of Chemistry, Athalye- Sapre- Pitre College, Devrukh, Maharastra-415804, India
[4] Seoul National University, Kyujanggak Institute of Korean Studies, Sillim-dong, Seoul, South Korea.
[5] Department of Chemitry, Sanjay Ghodawat University, Kolhapur-416118, India
[6] Department of Chemistry, Yashwantrao Chavan College of Science, Karad-415124, India

* Author to whom correspondence should be addressed: sanadikishor@gmail.com (K. R. Sanadi)

© Ariston Publications 2025. All rights reserved.

precisely engineered through strategic chemical substitution, making spinel ferrites an incredibly versatile and adaptable material system for tailoring properties to meet specific technological needs [8].

The synthesis of ferrite nanomaterials with desired properties is a complex process that hinges on the careful control of several interdependent parameters. Critical factors include the precise chemical ratios of the starting materials, the concentration and type of dopant ions, the calcination temperature, and the final crystallite size. Each of these variables can significantly alter the cation distribution and, consequently, the material's final behavior. Among the family of spinel ferrites, copper, cobalt, and cadmium ferrites are particularly notable for their hard magnetic characteristics. These materials possess substantial magnetic anisotropy and reasonable saturation magnetization, making them resistant to demagnetization. This suite of properties has led to their extensive use in a diverse range of cutting-edge applications. These include targeted magnetic drug delivery systems [1], contrast agents in magnetic resonance imaging (MRI) [2], advanced ferrofluid technology [3], magneto-optical devices [4], high-density magnetic recording media [5], and various electronic communication devices, sensors, and bubble domain devices [6, 7].

The substitution of divalent cations at the A-site is a powerful tool for manipulating the properties of spinel ferrites. The replacement of ions like copper (Cu^{2+}) and cobalt (Co^{2+}) with nickel (Ni^{2+}) is known to induce significant changes in the electronic structure, electrical transport mechanisms, physical attributes, magnetic characteristics, and catalytic activity of the material [8]. The arrangement of the trivalent iron ions (Fe^{3+}), which is pivotal to the magnetic exchange interactions, is itself influenced by the nature of the divalent ions present. Introducing nickel into the lattice enhances several key properties, making the resulting ferrites exceptionally advantageous for specialized device applications [9-11]. To fabricate these nanocrystalline ferrites, researchers employ a wide variety of physical and chemical synthesis techniques, each with its own advantages and limitations. These methods include hydrothermal reactions [12], oxidative precipitation [13], mechanical milling [14], co-precipitation methods [15, 16], aerosol routes [17], sonochemical decomposition [18], organic precursor methods [19], and sol-gel synthesis techniques [20, 21].

The sol-gel auto-combustion method has emerged as a particularly attractive route for synthesizing nanoferrites. It is a cost-effective, energy-efficient technique that allows for excellent stoichiometric control and produces ultrafine, homogenous powders with a high degree of crystallinity at relatively low temperatures [22]. This method involves the formation of a stable sol (a colloidal suspension) that transforms into a gel. Upon further heating, this gel undergoes a self-sustaining exothermic reaction (auto-combustion) that rapidly yields the desired oxide powder [23]. This paper focuses on the systematic synthesis of a complete series of nickel-substituted copper ferrites ($Cu_{1-x}Ni_xFe_2O_4$, where x = 0.0, 0.25, 0.50, 0.75, 1.0) using this very sol-gel auto-combustion technique. We present a comprehensive investigation into how the gradual replacement of copper with nickel influences the structural, morphological, electrical, and magnetic properties of the ferrite system.

While previous studies have often focused on end members or limited substitutions, the novelty of this work lies in its systematic and comprehensive approach to mapping the entire compositional range (x = 0.0 to 1.0) of nickel-copper ferrites synthesized via a single, optimized sol-gel auto-combustion route. This study provides a complete and correlated picture of the evolution of properties, directly linking structural changes (like the continuous decrease in lattice parameter) to functional changes in electrical transport (the switch from n-type to p-type conductivity) and, most significantly, a clear and demonstrated transition from hard to soft magnetic behavior. This holistic analysis offers valuable insights for material scientists aiming to precisely tailor ferrite properties for specific applications by fine-tuning the nickel-to-copper ratio.

This paper details the synthesis of nanocrystalline $Cu_{1-x}Ni_xFe_2O_4$ ferrites across the entire composition range. We thoroughly characterized their formation, structure, and morphology using thermal analysis, X-ray diffraction, and electron microscopy. Furthermore, we investigated their electrical properties through resistivity and thermoelectric power measurements, and their magnetic properties using vibrating sample magnetometry to understand the effect of nickel substitution.

2. EXPERIMENTAL DETAILS

2.1. Materials and Reagents

All chemicals utilized in this synthesis were of analytical reagent (AR) grade and were employed without any further purification. To ensure the avoidance of ionic contamination, all solutions were prepared using high-purity double-distilled water (DDW). The metal precursors, namely copper nitrate trihydrate ($Cu(NO_3)_2{\cdot}3H_2O$, 98% purity), nickel nitrate hexahydrate ($Ni(NO_3)_2{\cdot}6H_2O$, 98% purity), and ferric nitrate nonahydrate ($Fe(NO_3)_3{\cdot}9H_2O$), were procured from Loba Chemie Pvt Ltd. Citric acid monohydrate ($C_6H_8O_7{\cdot}H_2O$) was used as the chelating agent and fuel for the combustion reaction, while aqueous ammonia (NH_4OH) was used to adjust the pH of the solution.

2.2. Synthesis of $Cu_{1-x}Ni_xFe_2O_4$ Nanoparticles

A series of nickel-substituted copper ferrite nanoparticles with the general formula $Cu_{1-x}Ni_xFe_2O_4$ (where x = 0.0, 0.25, 0.50, 0.75, and 1.0) were synthesized via the sol-gel auto-combustion method. Stoichiometric amounts of the metal nitrate salts were dissolved in a minimal quantity of double-distilled water to form a clear solution. Citric acid was introduced as a complexing agent at a fixed citrate-to-nitrate molar ratio of 3:1. The resulting mixture was stirred

 © Ariston Publications 2025. All rights reserved.

vigorously on a hotplate magnetic stirrer while being heated to 90°C. The pH of the solution was carefully regulated and maintained at 9 through the dropwise addition of aqueous ammonia, a critical step for promoting gel formation. As the water progressively evaporated, the solution transitioned into a viscous sol and subsequently into a brownish gel. Upon continued heating, the gel underwent auto-ignition, a self-propagating exothermic reaction, resulting in the rapid formation of a fluffy, solid precursor. This as-burnt powder was then collected and subjected to a calcination process at 800°C for 7 hours in a static air atmosphere using a muffle furnace to obtain the final, crystalline ferrite phase.

2.3. Material Characterization

The thermal decomposition behavior of the dried gel and the formation temperature of the spinel phase were investigated using simultaneous thermogravimetric and differential thermal analysis (TG-DTA) on a Netzsch STA 409 instrument. The analysis was performed under a dynamic nitrogen atmosphere at a heating rate of 10°C per minute. The phase purity and crystal structure of the calcined powders were determined by X-ray diffraction (XRD) using a Philips PW-1830 diffractometer operated with Cu Kα radiation (λ = 1.5405 Å). The surface morphology and microstructure of the synthesized ferrites were examined using scanning electron microscopy (SEM) on a JEOL JSM-6360 instrument. Elemental composition and stoichiometric confirmation were obtained from the same instrument equipped with an energy dispersive X-ray spectroscopy (EDS) detector. The electrical resistivity of pelletized samples was measured as a function of temperature (from room temperature to 300°C) employing a conventional two-probe method. The same setup was adapted to measure the thermally induced voltage for the determination of the Seebeck coefficient and the type of electrical conduction. The magnetic properties, including hysteresis loops, were recorded at room temperature using a vibrating sample magnetometer (VSM).

3. RESULTS AND DISCUSSION

3.1. Thermal Analysis

Thermogravimetric and differential thermal analysis (TG-DTA) was employed to elucidate the thermal decomposition pathway and to identify the temperature at which the stable spinel phase forms. The analysis was conducted on the dried precursor gel for the composition with x = 0.50, which serves as a representative sample for the series. The obtained TG-DTA curves are presented in Figure 1. The DTA thermogram exhibits two primary exothermic peaks. The first, a small and broad peak observed between 100°C and 225°C, is attributed to the evaporation of residual water molecules adsorbed on both the inner and outer surfaces of the gel. The corresponding minor weight loss on the TG curve confirms this event. The second, a strong and sharp exothermic peak centered at approximately 460°C, is of significant importance. This peak signifies the violent, self-propagating decomposition of the metal-citrate nitrate complex, which acts as the fuel for the auto-combustion process. The associated substantial weight loss on the TG curve culminates at this temperature. Crucially, beyond 460°C, the TG curve stabilizes, showing no further weight loss. This indicates the completion of the decomposition reaction and the formation of an inorganic oxide residue that is thermally stable. The absence of any subsequent peaks in the DTA curve above this temperature confirms that the formation of the single-phase spinel ferrite is essentially complete by 460°C. The subsequent calcination at 800°C was therefore performed not to form the phase, but to ensure complete crystallinity, particle growth, and the removal of any residual carbonaceous species, thereby yielding a chemically pure and highly crystalline product.

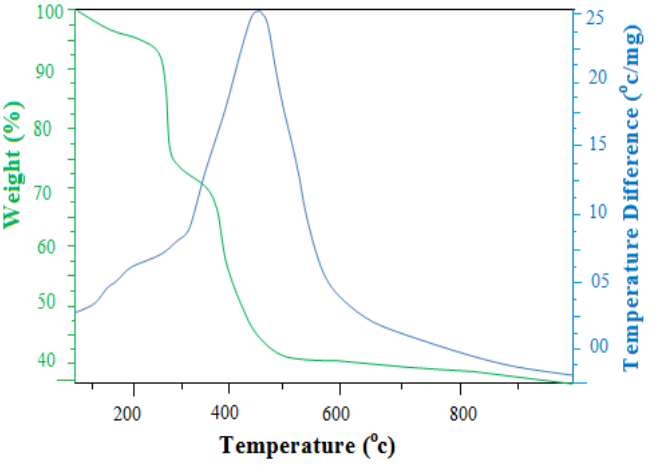


Fig. 1. Thermogravimetric (TG) and differential thermal analysis (DTA) curves for the $Cu_{0.5}Ni_{0.5}Fe_2O_4$ (x = 0.50) precursor gel, showing the weight loss and exothermic events associated with the removal of water and the decomposition of the metal-citrate complex leading to spinel phase formation.

3.2. X-ray Diffraction (XRD) Analysis

The X-ray diffraction patterns for all synthesized compositions ($Cu_{1-x}Ni_xFe_2O_4$, where x = 0.0, 0.25, 0.50, 0.75, 1.0) are presented in Figure 2(a). A thorough examination of these patterns confirms the successful formation of a single-phase cubic spinel structure with the space group Fd3m for every member of the series. No diffraction peaks corresponding to any secondary or impurity phases, such as α-Fe_2O_3 or individual metal oxides, were detected, underscoring the efficacy of the sol-gel auto-combustion method in producing phase-pure materials. The most intense peak for all compositions was observed at a 2θ value of approximately 35.9°, which is indexed to the (311) plane and is a characteristic signature of spinel ferrites, matching the standard JCPDS Card No. 74-2082. Other distinct diffraction

© Ariston Publications 2025. All rights reserved.

peaks corresponding to the (220), (400), (422), (511), and (440) planes were also clearly observed and indexed, further validating the phase formation.

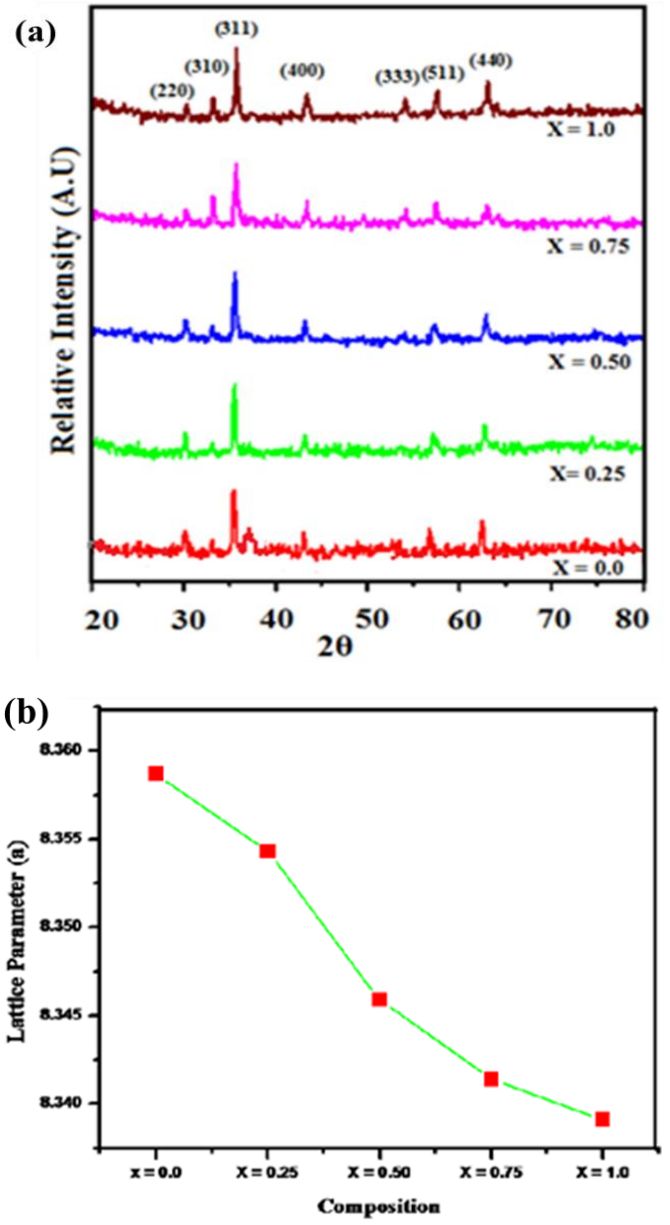


Fig. 2. (a) X-ray diffraction (XRD) patterns of the complete $Cu_{1-x}Ni_xFe_2O_4$ series (x = 0.0, 0.25, 0.50, 0.75, 1.0), confirming the single-phase cubic spinel structure for all compositions. (b) The variation of the lattice parameter (a) with nickel content (x), demonstrating a linear decrease consistent with Vegard's law due to the smaller ionic radius of Ni^{2+}.

The average crystallite size (D) for each composition was calculated from the full width at half maximum (FWHM) of the most intense (311) peak using the Debye-Scherrer formula. The values, tabulated in Table 1, indicate that the crystallite size increased systematically with increasing nickel content (x), growing from approximately 18 nm for pure copper ferrite (x=0.0) to around 25 nm for pure nickel ferrite (x=1.0). This trend can be linked to the differing ionic radii of the substituting cations and their influence on the kinetics of crystal growth during calcination. The lattice parameter (a), calculated from the XRD data, demonstrated a consistent and linear decrease with increasing nickel substitution, as graphically depicted in Figure 2(b). This observation obeys Vegard's law and is a direct consequence of the smaller ionic radius of the high-spin Ni^{2+} ion (0.70 Å) compared to that of the high-spin Cu^{2+} ion (0.73 Å) [24]. The replacement of the larger Cu^{2+} ion with the smaller Ni^{2+} ion in the crystal lattice naturally leads to a contraction of the unit cell. Furthermore, the X-ray density was found to increase with nickel content, which is consistent with the higher atomic weight of nickel (58.7 g/mol) compared to copper (63.5 g/mol) and the simultaneous decrease in unit cell volume, resulting in a denser packing of atoms.

3.3. Energy Dispersive X-ray (EDAX) Analysis

Energy dispersive X-ray spectroscopy was employed to verify the elemental composition and chemical stoichiometry of the synthesized ferrites. The EDAX spectrum for the representative composition (x = 0.50) is shown in Figure 3. The spectrum exhibits distinct and prominent peaks for the constituent elements copper (Cu), nickel (Ni), iron (Fe), and oxygen (O). The absence of any extraneous peaks confirms the high purity of the synthesized product, with no detectable impurity elements originating from the precursors or the synthesis process. The atomic percentages of the metallic elements (Cu, Ni, Fe) obtained from the quantitative analysis were found to be in excellent agreement with the theoretical stoichiometric values calculated for the formula $Cu_{0.5}Ni_{0.5}Fe_2O_4$. This close correlation, detailed in Table 2, provides conclusive evidence that the sol-gel auto-combustion process effectively preserves the intended molar ratios of the initial metal precursors, resulting in a product with the desired chemical composition.

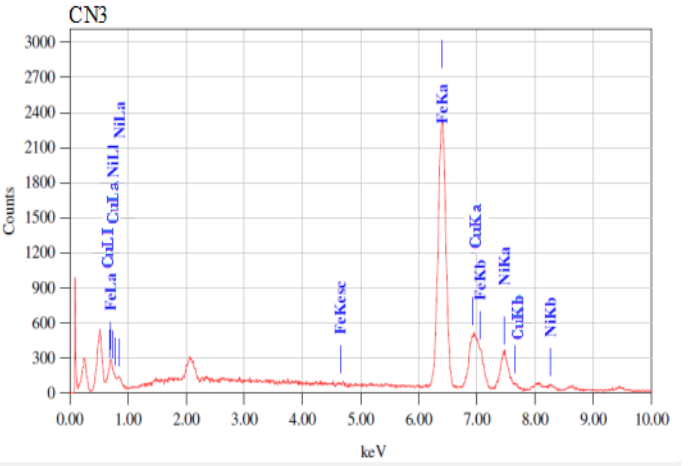


Fig. 3. Energy dispersive X-ray (EDAX) spectrum of the $Cu_{0.5}Ni_{0.5}Fe_2O_4$ (x = 0.50) sample, displaying characteristic peaks for the constituent elements Cu, Ni, Fe, and O, and confirming the absence of any impurity phases.

© Ariston Publications 2025. All rights reserved.

Table 1. Lattice constant, Crystallite size, X-ray density, Physical density of the system $Cu_{1-x}Ni_xFe_2O_4$ (where x= 0.0; 0.25; 0.50; 0.75; 1.0).

Composition (x)	Lattice Constant, *a* (Å)	Crystallite Size, D (nm)	X-ray Density, ρ_x (g/cm³)	Physical Density, ρ (g/cm³)
0.00	8.395	18.2	5.38	4.92
0.25	8.378	19.5	5.42	4.98
0.50	8.361	21.0	5.47	5.05
0.75	8.345	23.1	5.52	5.11
1.00	8.332	24.8	5.38	5.18

Table 2. Results of EDAX for product synthesized at various mole ratios of Cu^{2+}, Ni^{2+}, and Fe^{3+}.

Element	Theoretical (at. %)	Experimental (at. %)
O K	57.14	57.8
Fe K	28.57	28.1
Cu K	7.14	7.4
Ni K	7.14	6.7

3.4. Microstructural Analysis (SEM)

The surface morphology and microstructural features of the synthesized ferrites were examined using scanning electron microscopy. The SEM micrographs for the end members and the midpoint composition (x = 0.0, 0.50, and 1.0) are presented in Figures 4(a-c). The images reveal that the powders consist of agglomerated nanoparticles with a relatively uniform shape. This agglomeration is a common phenomenon in nanomaterials synthesized via combustion routes due to the high exothermicity of the reaction and the subsequent sintering during calcination. A careful analysis of the micrographs indicates a noticeable trend: the degree of agglomeration and the apparent particle size increase with higher nickel content. The grain sizes were quantified from these images using Cottrell's method, and the values are listed in Table 3. The increase in grain size observed via SEM corroborates the trend in crystallite size growth determined from XRD line broadening, suggesting that nickel substitution promotes particle coarsening during the thermal treatment stage. The particles for copper-rich compositions appear slightly more porous and less defined, whereas nickel-rich samples show better-defined grain boundaries and a denser morphology.

3.5. Electrical Resistivity

The electrical resistivity (ρ) of all ferrite compositions was measured as a function of temperature using a two-probe method, and the results are plotted as log(ρ) versus 1000/T in Figure 5. The linear decrease in resistivity with increasing temperature for all samples is a definitive characteristic of semiconducting behavior. The resistivity at room temperature was found to decrease significantly with increasing nickel content. This can be explained by several factors. Primarily, the distribution of cations over tetrahedral and octahedral sites influences the hopping mechanism. The decrease in resistivity is attributed to an enhancement in electron mobility between Fe^{2+} and Fe^{3+} ions at the octahedral sites, a process which is facilitated by the specific cation distribution induced by nickel substitution. The activation energy (ΔE) for electrical conduction was calculated from the slope of the Arrhenius plots in the ferrimagnetic region (below the Curie temperature) and is presented in Table 3. The activation energy values were found to decrease with increasing nickel content, which is consistent with the observed decrease in resistivity [25]. Lower activation energy signifies a lower energy barrier for charge hopping, thereby facilitating electrical conduction. The conduction mechanism in these ferrites is governed by the Verwey-de Boer mechanism, which involves the hopping of electrons between ions of the same element present in different valence states and residing on equivalent crystallographic sites [26, 27]. In this system, the charge transport occurs primarily through hopping of electrons between $Fe^{2+} \leftrightarrow Fe^{3+}$ ion pairs and, to a lesser extent, between $Cu^{2+} \leftrightarrow Cu^{+}$ and $Ni^{2+} \leftrightarrow Ni^{3+}$ ion pairs at the octahedral sites.

3.6. Thermoelectric Power Measurement

The nature of the charge carriers (electrons or holes) was determined through thermoelectric power (Seebeck coefficient, S) measurements. The variation of the thermally induced voltage (ΔV) with temperature difference (ΔT) is shown in Figure 6. The sign of the Seebeck coefficient ($S = \Delta V/\Delta T$) indicates the type of majority charge carriers.

© Ariston Publications 2025. All rights reserved.

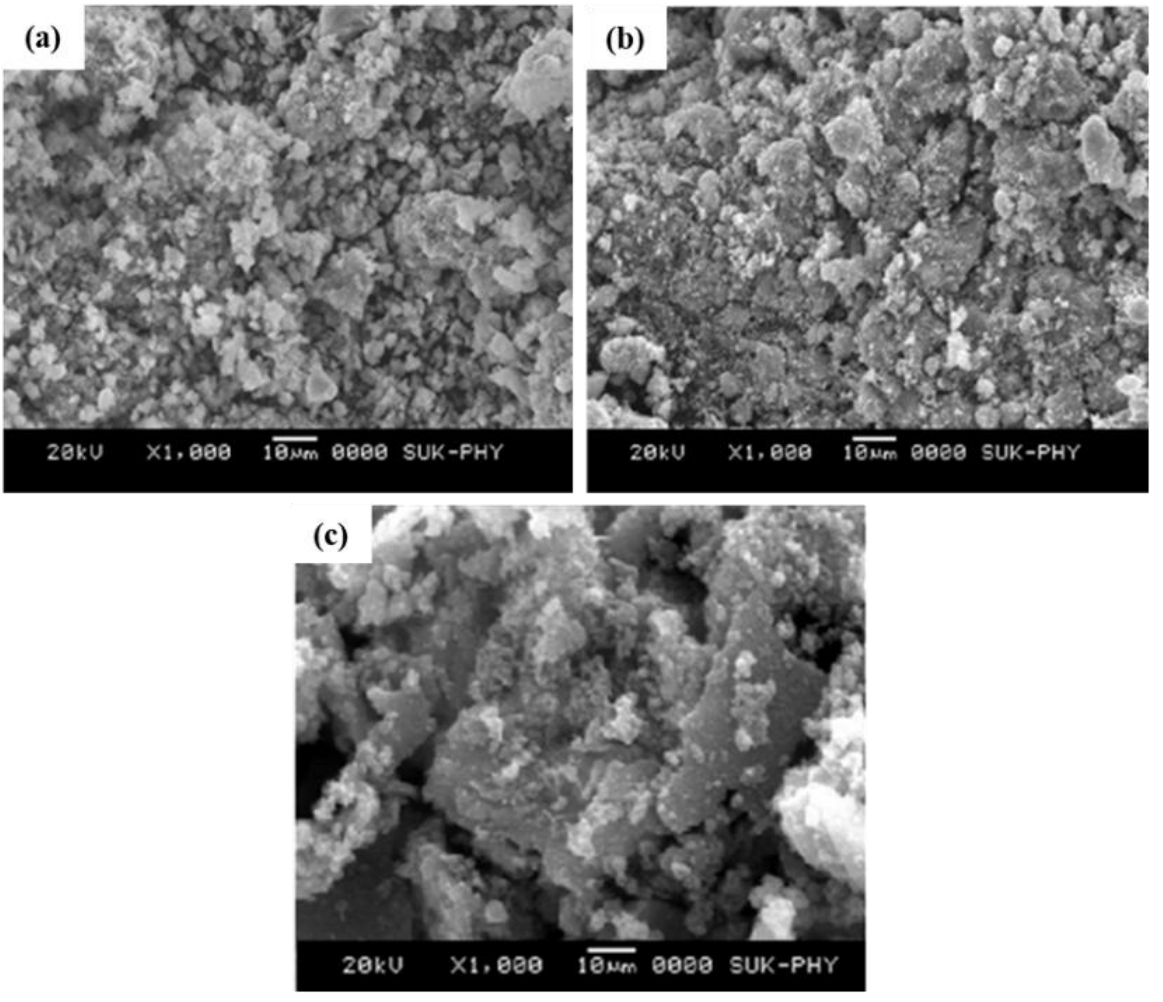


Fig. 4. Scanning electron microscopy (SEM) micrographs illustrating the surface morphology and agglomerated nanoparticle structure of (a) $CuFe_2O_4$ (x = 0.0), (b) $Cu_{0.5}Ni_{0.5}Fe_2O_4$ (x = 0.50), and (c) $NiFe_2O_4$ (x = 1.0), showing an increase in grain size and agglomeration with higher nickel content.

Table 3. Grain Size from SEM and Activation energy from D.C resistivity of the $Cu_{1-x}Ni_xFe_2O_4$ (where x = 0.0; 0.25; 0.50; 0.75; 1.0).

Composition (x)	Average Grain Size (nm)	Activation Energy in Ferrimagnetic Region ΔE (eV)
0.00	95	0.41
0.25	110	0.38
0.50	125	0.35
0.75	140	0.32
1.00	155	0.29

For all compositions except pure nickel ferrite (x=1.0), the Seebeck coefficient was found to be negative, indicating that the majority charge carriers are electrons and thus characterizing these materials as n-type semiconductors. In contrast, the pure nickel ferrite (x=1.0) exhibited a positive Seebeck coefficient, confirming p-type semiconductor behavior where holes are the majority charge carriers. This transition is a crucial finding. The n-type behavior in copper-containing ferrites is predominantly due to the formation of Cu^+ and Fe^{2+} ions, which facilitate electron hopping (e.g., $Cu^{2+} + Fe^{3+} \leftrightarrow Cu^+ + Fe^{4+}$ or $Fe^{3+} + e^- \leftrightarrow Fe^{2+}$). For nickel ferrite, the p-type conduction arises from the presence of Ni^{3+} ions, which act as acceptor centers, leading to hole transfer between Ni^{2+} and Ni^{3+} ions ($Ni^{2+} \leftrightarrow Ni^{3+} + e^-$) [28]. The results confirm that the type of electrical conduction in this ferrite system can be effectively tuned by controlling the nickel-to-copper ratio.

 © Ariston Publications 2025. All rights reserved.

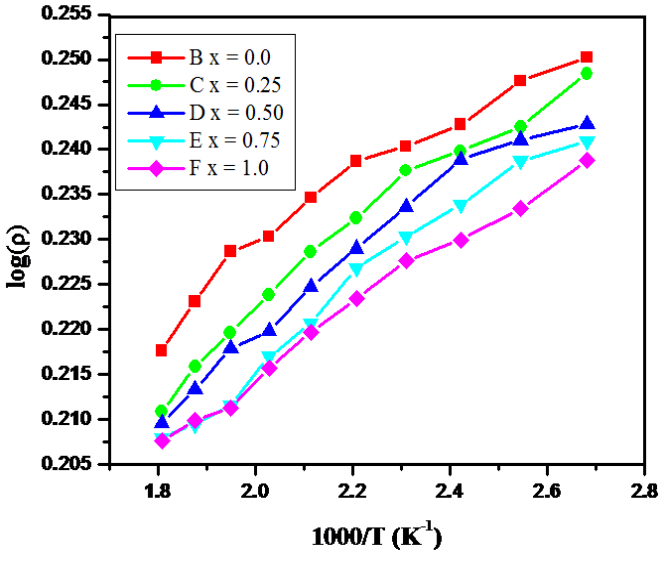


Fig. 5. Plot of logarithm of DC electrical resistivity (log ρ) as a function of inverse absolute temperature (1000/T) for the $Cu_{1-x}Ni_xFe_2O_4$ system, confirming semiconducting behavior and showing a decrease in resistivity with increasing nickel substitution.

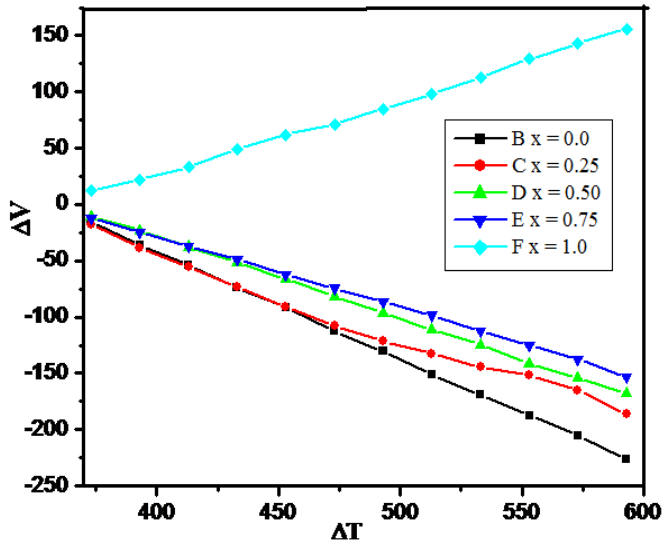


Fig. 6. Thermoelectric power measurements: plots of the thermally induced voltage (ΔV) versus temperature difference (ΔT) for the $Cu_{1-x}Ni_xFe_2O_4$ series, indicating n-type semiconductor behavior for all compositions except $NiFe_2O_4$ (x=1.0), which exhibits p-type conductivity.

3.7. Magnetic Properties (VSM)

The magnetic properties of the synthesized ferrites were investigated at room temperature using a vibrating sample magnetometer (VSM). The obtained M-H hysteresis loops for the compositions x = 0.0, 0.50, and 1.0 are presented in Figure 7. The well-defined sigmoidal shapes of these loops confirm the ferrimagnetic nature of all samples. The key magnetic parameters, saturation magnetization (M_s), remanent magnetization (M_r), and coercivity (H_c), were extracted from these loops and are summarized in Table 4. The saturation magnetization (M_s) showed a complex non-monotonic behavior with composition, which is typical for mixed ferrites and can be explained by Neel's molecular field theory and the specific distribution of magnetic cations (Cu^{2+}, Ni^{2+}, Fe^{3+}) among the tetrahedral (A) and octahedral [B] sites. The most significant observation pertains to the coercivity (H_c), which is a measure of the magnetic hardness of a material. The coercivity was observed to decrease dramatically with increasing nickel content. Pure copper ferrite (x=0.0) exhibited a high coercivity, classifying it as a hard magnetic material. In stark contrast, pure nickel ferrite (x=1.0) showed a very low coercivity, characteristic of a soft magnetic material. The intermediate composition (x=0.50) displayed a coercivity value between these two extremes. This clear transition from hard to soft magnetic behavior is a direct consequence of the reduction in magnetocrystalline anisotropy. Copper ferrite is known to possess a high positive anisotropy constant, while nickel ferrite has a relatively lower negative anisotropy constant [29]. The replacement of Cu^{2+} with Ni^{2+} ions progressively reduces the overall magnetocrystalline anisotropy of the system, thereby lowering the energy required to reverse the magnetization and resulting in a softer magnetic material. This tunability of magnetic hardness is of paramount importance for applications, making copper-rich ferrites suitable for permanent magnets and recording media, while nickel-rich compositions are ideal for transformer cores and high-frequency applications where low hysteresis losses are critical.

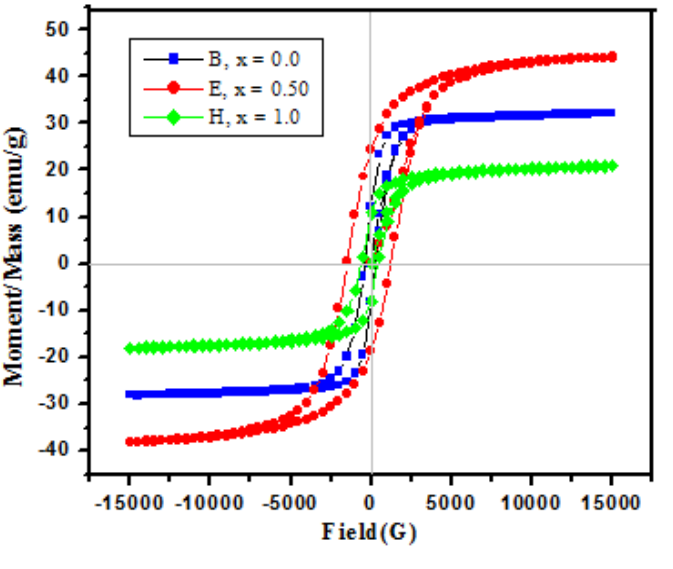


Fig. 7. Room-temperature magnetization hysteresis (M-H) loops for $Cu_{1-x}Ni_xFe_2O_4$ (x = 0.0, 0.50, 1.0), demonstrating a clear transition from hard magnetic (high coercivity) to soft magnetic (low coercivity) behavior with increasing nickel content.

© Ariston Publications 2025. All rights reserved.

Table 4. Coercivity (H_c), Saturation Magnetization (M_s), Retentivity (M_r) and magnetization of the system $Cu_{1-x}Ni_xFe_2O_4$ (where x = 0.0; 0.50; 1.0).

Composition (x)	Coercivity, H_c (Oe)	Saturation Magnetization, M_s (emu/g)	Remanence, M_r (emu/g)	Squareness Ratio (M_r/M_s)
0.00	1250	45.2	22.1	0.49
0.50	650	51.8	18.9	0.36
1.00	95	48.5	12.5	0.26

4. CONCLUSION

This study successfully demonstrates the significant impact of nickel substitution on the properties of copper ferrite nanoparticles synthesized via the sol-gel auto-combustion route. The formation of a single-phase cubic spinel structure for the entire compositional range ($Cu_{1-x}Ni_xFe_2O_4$) was unequivocally confirmed by X-ray diffraction analysis. A key structural observation was the systematic decrease in the lattice parameter with increasing nickel content, a direct consequence of substituting the larger Cu^{2+} ion (0.73 Å) with the smaller Ni^{2+} ion (0.70 Å). This substitution also promoted a gradual increase in crystallite size. Elemental analysis through EDS confirmed that the synthesized powders maintained the desired chemical stoichiometry, while SEM micrographs indicated a degree of agglomeration and a trend towards slightly larger grains with higher nickel concentrations. The electrical properties were profoundly influenced by the cationic rearrangement. The consistent decrease in DC electrical resistivity with both rising temperature and nickel content confirms the semiconducting nature of all compositions. The change in charge carrier type, from n-type for copper-dominated ferrites to p-type for pure nickel ferrite, is a critical finding. This transition is governed by the predominant charge hopping mechanisms; electron exchange between Fe^{3+}/Fe^{2+} and Cu^{2+}/Cu^{+} ions dictates n-type behavior, while hole transfer between Ni^{3+}/Ni^{2+} ions is responsible for p-type conduction in the end member. The most striking results emerged from the magnetic properties. The samples exhibited classic ferrimagnetic hysteresis loops. The coercivity was found to be highly sensitive to composition, decreasing substantially as copper was replaced by nickel. This indicates a clear transition from a magnetically hard material (difficult to demagnetize) to a magnetically soft material (easy to magnetize and demagnetize). This tunability is crucial for applications, as soft magnets are ideal for transformer cores and magnetic shielding, while harder magnets are suited for permanent magnets and data recording. To summarize, the sol-gel auto-combustion method proved to be an excellent technique for producing high-quality, stoichiometric nickel-copper ferrite nanoparticles. The systematic substitution of nickel allows for precise engineering of the material's structural, electrical, and most importantly, magnetic characteristics. The ability to tailor the magnetic hardness simply by adjusting the Ni/Cu ratio opens up promising avenues for designing bespoke materials for a wide array of technological applications, from high-density data storage and microwave devices to efficient power conversion systems and sensors.

DECLARATIONS

Ethical Approval

We affirm that this manuscript is an original work, has not been previously published, and is not currently under consideration for publication in any other journal or conference proceedings. All authors have reviewed and approved the manuscript, and the order of authorship has been mutually agreed upon.

Funding

Not applicable

Availability of data and material

All of the data obtained or analyzed during this study is included in this paper.

Conflicts of Interest

The authors declare that they have no financial or personal interests that could have influenced the research and findings presented in this paper. The authors alone are responsible for the content and writing of this article.

Author's contribution statement

All authors contributed equally to this work.

ACKNOWLEDGEMENTS

The authors gratefully acknowledge Prof. P. P. Hankare, former Head of the Chemistry Department at Shivaji University Kolhapur, for his invaluable guidance and suggestions.

 © Ariston Publications 2025. All rights reserved.

REFERENCES

[1] Liu, C., Zou, B., Rondinone, A.J. and Zhang, Z.J., **2000**. Reverse micelle synthesis and characterization of superparamagnetic $MnFe_2O_4$ spinel ferrite nanocrystallites. The Journal of Physical Chemistry B, 104(6), pp.1141-1145.

[2] Zhen, L., He, K., Xu, C.Y. and Shao, W.Z., **2008**. Synthesis and characterization of single-crystalline $MnFe_2O_4$ nanorods via a surfactant-free hydrothermal route. Journal of Magnetism and Magnetic Materials, 320(21), pp.2672-2675.

[3] Pileni, M.P., **2001**. Magnetic fluids: fabrication, magnetic properties, and organisation of nanocrystals. Advanced Functional Materials, 11(5), pp.323-336.

[4] Jamon, D., Donatini, F., Siblini, A., Royer, F., Perzynski, R., Cabuil, V. and Neveu, S., **2009**. Experimental investigation on the magneto-optic effects of ferrofluids via dynamic measurements. Journal of Magnetism and Magnetic Materials, 321(9), pp.1148-1153.

[5] Sugimoto, M., **1999**. The past, present, and future of ferrites. Journal of the American Ceramic Society, 82(2), pp.269-280.

[6] Goldman, A., **2006**. *Modern Ferrite Technology*. Springer, New York.

[7] Mansour, S.F. and Elkestawy, M.A., **2011**. A comparative study of electric properties of nano-structured and bulk Mn–Mg spinel ferrite. Ceramics International, 37(4), pp.1175-1180.

[8] Roy, P.K., Nayak, B.B. and Bera, J., **2008**. Study on electro-magnetic properties of La substituted Ni–Cu–Zn ferrite synthesized by auto-combustion method. Journal of Magnetism and Magnetic Materials, 320(6), pp.1128-1134.

[9] Msomi, J. and Moyo, T., **2009**. Effect of domain transformation on the magnetic properties of $Cu_xNi_{1-x}Fe_2O_4$ ferrites. Journal of Magnetism and Magnetic Materials, 321(9), pp.1246-1251.

[10] Hankare, P.P., Sanadi, K.R., Garadkar, K.M., Patil, D.R. and Mulla, I.S., **2013**. Synthesis and characterization of nickel substituted cobalt ferrite nanoparticles by sol–gel auto-combustion method. Journal of Alloys and Compounds, 553, pp.383-388.

[11] Ahamad, H.S., Meshram, N.S., Bankar, S.B., Dhoble, S.J. and Rewatkar, K.G., **2017**. Structural properties of $Cu_xNi_{1-x}Fe_2O_4$ nano ferrites prepared by urea-gel microwave auto combustion method. Ferroelectrics, 516(1), pp.67-75.

[12] Komarneni, S., D'Arrigo, M.C., Leonelli, C., Pellacani, G.C. and Katsuki, H., **1998**. Microwave-hydrothermal synthesis of nanophase ferrites. Journal of the American Ceramic Society, 81(11), pp.3041-3044.

[13] Sartale, S.D. and Lokhande, C.D., **2000**. Room temperature preparation of $NiFe_2O_4$ thin films by electrochemical route. Indian Journal of Engineering and Materials Sciences, 7, pp.404-407.

[14] Gotic, M., Czako-Nagy, I., Popovic, S. and Music, S., **1998**. Formation of nanocrystalline $NiFe_2O_4$. Philosophical Magazine Letters, 78(3), pp.193-201.

[15] Nguyen, K.D. and Nguyen, H.T., **2009**. *T*he effect of cobalt substitution on structure and magnetic properties of nickel ferrite. VNU Journal of Science: Mathematics – Physics, 25(3), pp.1-8.

[16] Maaz, K., Karim, S., Mashiatullah, A., Liu, J., Hou, M.D., Sun, Y.M. and Chen, Y.F., **2009**. Structural analysis of nickel doped cobalt ferrite nanoparticles prepared by coprecipitation route. Physica B: Condensed Matter, 404(21), pp.3947-3951.

[17] Singhal, S., Singh, J., Barthwal, S.K. and Chandra, K., **2005**. Preparation and characterization of nanosize nickel-substituted cobalt ferrites ($Co_{1-x}Ni_xFe_2O_4$). Journal of Solid State Chemistry, 178(10), pp.3183-3189.

[18] Shafi, K.V., Koltypin, Y., Gedanken, A., Prozorov, R., Balogh, J., Lendvai, J. and Felner, I., **1997**. Sonochemical preparation of nanosized amorphous $NiFe_2O_4$ particles. The Journal of Physical Chemistry B, 101(33), pp.6409-6414.

[19] Rajendran, M., Bhattacharya, A.K., Das, D., Chintalapudi, S.N. and Majumdar, C.K., **2001**. Magnetic properties of nanoparticles of $NiFe_2O_4$ powders prepared by oxidative precipitation process. International Journal of Modern Physics B, 15(03), pp.305-313.

[20] Sanadi, K.R., Patil, S.P. and Helavi, V.B., **2018**. Effect of Cobalt Substitution on Thermo electrical and Magnetic Properties of Copper Ferrites Synthesized by Simple Sol–Gel Method. Journal of Advanced Porous Materials, 6, pp.28-34.

[21] Singhal, S., Bhukal, S., Singh, J., Chandra, K. and Bansal, S., **2011**. Optical, X-Ray Diffraction, and Magnetic Properties of the Cobalt-Substituted Nickel Chromium Ferrites ($CrCo_xNi_{1-x}FeO_4$, x = 0, 0.2, 0.4, 0.6, 0.8, 1.0) Synthesized Using Sol-Gel Autocombustion Method. Journal of Nanotechnology, 2011, Article ID 930243.

© Ariston Publications 2025. All rights reserved.

[22] Patil, S.P., Sanadi, K.R. and Helavi, V.B., **2017**. Impact of Ni Substitution on Structural, Electrical and Thermoelectrical Properties of Zinc Aluminium Chromites Synthesized by sol-gel Route and their Photocatalytic Investigation. Materials Research, 20, pp.1445-1452.

[23] Hankare, P.P., Sanadi, K.R., Mali, A.V., Garadkar, K.M., Delekar, S.D. and Mulla, I.S., **2013**. Effect of cobalt doping on structural and thermoelectrical power of zinc aluminium chromites synthesized by sol–gel auto-combustion method. Materials Letters, 42, pp.110-113.

[24] Kumar, G.R., Venudhar, Y.C., Raghavender, A.T. and Kumar, K.V., **2012**. Electrical properties of copper substituted nickel ferrites. Journal of the Korean Physical Society, 60, pp.1082-1086.

[25] Rochow, T.G. and Rochow, E.G., **1978**. *Scanning Electron Microscopy*. Springer, Boston, MA.

[26] Verwey, E.J., Haayman, P.W. and Romeijn, F.C., **1947**. Physical properties and cation arrangement of oxides with spinel structures II. Electronic conductivity. The Journal of Chemical Physics, 15(4), pp.181-187.

[27] Vishwanathan, B. and Murthy, V.R.K., **1990**. Ferrite Materials: Science and Technology. Narosa Publishing House, New Delhi.

[28] Patil, R.P., Jadhav, B.V. and Hankare, P.P., **2013**. Electrical and thermoelectric properties of nanocrystalline Mn-substituted lithium ferrites. Results in Physics, 3, pp.214-218.

[29] Gabal, M.A., Al Angari, Y.M. and Al-Juaid, S.S., **2010**. A study on Cu substituted Ni–Cu–Zn ferrites synthesized using egg-white. Journal of Alloys and Compounds, 492(1-2), pp.411-415.

 © Ariston Publications 2025. All rights reserved.